Postsynaptic receptors regulate presynaptic transmitter stability through trans-synaptic bridges

Swetha K. Godavarthi[1,2*], Masaki Hiramoto[3], Yuri Ignatyev[4], Jacqueline B. Levin[5], Hui-quan Li[1,2], Marta Pratelli[1,2], Jennifer Borchardt[6], Cynthia Czajkowski[6], Laura N. Borodinsky[5], Lora Sweeney[4], Hollis T. Cline[3], Nicholas C. Spitzer[1,2*]

[1]Neurobiology Department, University of California San Diego, USA

[2]Kavli Institute for Brain & Mind, University of California San Diego, USA

[3]Neuroscience Department, The Scripps Research Institute, La Jolla CA, USA

[4]Institute of Science and Technology Austria, Austria

[5]Department of Physiology & Membrane Biology, Shriners Hospital for Children, Northern California; University of California Davis, School of Medicine, USA

[6]Neuroscience Department, University of Wisconsin Madison, USA

Abstract

Stable matching of neurotransmitters with their receptors is fundamental to synapse function, to achieve reliable and robust communication in neural circuits. Presynaptic neurotransmitters regulate selection of postsynaptic transmitter receptors. However, whether postsynaptic receptors regulate selection of presynaptic transmitters is unknown. Here we show that blockade of postsynaptic acetylcholine receptors at the neuromuscular junction leads to loss of the cholinergic phenotype in motor neurons and stabilization of an earlier, developmentally transient glutamatergic phenotype. Exogenous postsynaptic expression of $GABA_A$ receptors leads to the stabilization of an earlier, developmentally transient GABAergic motor neuron phenotype. Both acetylcholine receptors and GABA

receptors are linked to presynaptic neurons through trans-synaptic bridges. Knock-down of different components of these trans-synaptic bridges prevents stabilization of the cholinergic and GABAergic phenotypes. We conclude that this bidirectional communication enforces a match between transmitter and receptor and ensures the fidelity of synaptic transmission. Our findings suggest a role of dysfunctional transmitter receptors in neurological disorders that involve the loss of the presynaptic transmitter.

Main

Postsynaptic receptors at neuronal synapses are often viewed as passive responders to presynaptic neurotransmitters. For example, dendrites respond to uncaged glutamate or GABA by forming spines that express glutamate or GABA receptors[1,2], filopodia respond to release of glutamate from developing axons, leading to physiological and morphological maturation[3] , and cultured glutamatergic neurons form functional glutamatergic synapses with skeletal muscle cells[4] . Also, when neurotransmitters switch, the postsynaptic cell responds to the newly expressed transmitter by expressing a matching receptor[5–8]. Activity-driven retrograde signaling by endocannabinoids and neurotrophins from the postsynapse regulates presynaptic neuron survival, dendrite formation and growth, and synaptogenesis[9,10]. Do changes in the receptors on postsynaptic cells alter transmitter expression in their presynaptic neurons? Here we demonstrate that retrograde signaling by postsynaptic transmitter receptors is necessary and sufficient to stabilize expression of their cognate transmitter in presynaptic neurons and that signaling is blocked by disruption of trans-synaptic bridges.

Blocking endogenous acetylcholine receptors at the neuromuscular junction

46 We first tested whether blockade of acetylcholine receptors (AChR) of cholinergic neuromuscular
47 junctions in *Xenopus* embryos affects the expression of acetylcholine in motor neurons. Agarose
48 beads containing AChR antagonists, pancuronium or curare, were implanted into developing
49 mesoderm at 1 day post fertilization (dpf) for local, diffusive drug delivery (**Fig. 1a**). Larvae were
50 wholemount immunostained for choline acetyltransferase (ChAT), the enzyme that synthesizes
51 ACh, and for synaptic vesicle protein 2 (SV2), a marker of nerve terminals, to determine the
52 capacity of nerve terminals for ACh synthesis. At 2 dpf, the staining of terminals running along
53 the myocommatal junctions at the boundaries between chevrons of myocytes was not different
54 from the staining in saline bead controls (**Fig. 1b** and **1e**). By 3 dpf, the staining for ChAT had
55 decreased to 19% of controls with no change in staining for SV2 (**Fig. 1c** and **1e**). By 4 dpf the
56 staining for ChAT had fallen to 5% of controls (**Fig. 1d** and **1e**), while SV2 staining was 73% of
57 controls (**Fig. 1e**; **Suppl Figs. 1, 2, 3 and Suppl Table 1**). These results indicate that the loss of
58 ChAT precedes the loss of nerve terminals and suggest that blockade of postsynaptic AChR
59 impairs the stability of ChAT expression. This finding is consistent with the observation of a
60 decrease in the presynaptic active zone protein Bruchpilot, associated with presynaptic transmitter
61 synthesis and release[11], following blockade of postsynaptic receptor subunits[12] that occurs early in
62 homeostatic presynaptic scaling[13,14]. The decrease is reversed only when the receptor function is
63 restored by expression and insertion of a different, reserve receptor subunit[14,15]. In the present case,
64 the absence of reserve receptor subunits of the skeletal muscle ACh receptor[16] facilitated
65 identification of the postsynaptic receptor-dependence of presynaptic transmitter stability.
66 Interestingly, the loss of AChR precedes the loss of nerve terminals in a mouse model of
67 myasthenia gravis (MG)[17]. MG is often the result of an autoimmune attack on AChR function[18–
68 20]. Our findings suggest that reduced levels of presynaptic ACh, in addition to loss of AChR,

69 contribute to the ensuing muscle fatigue that is also observed in congenital MG resulting from
70 ChAT deficiency[19].
71
72 Normally, embryonic *Xenopus* motor neurons express glutamate in their cell bodies at 1 dpf and
73 its level decreases by 2 dpf as ChAT begins to be detected[21]. By 3 dpf glutamate is no longer
74 detected immunohistochemically. Blockade of AChR with pancuronium led to increased
75 expression of a vesicular glutamate transporter (VGLUT1) in motor neuron terminals (**Fig. 1f**;
76 **Suppl Fig. 4**), suggesting the stabilization of a glutamatergic phenotype. The expression of
77 VGLUT1 was accompanied by a corresponding increase in expression of glutamatergic AMPA
78 and NMDA receptor subunits in myocytes (**Fig. 1, g** and **h**). Intracellular recordings from these
79 myocytes at 4 dpf yielded two classes of miniature endplate potentials (mEPPs), recognized by
80 their rise and decay times (**Fig. 1, i** to **r**) and their frequency, with a mean frequency overall of
81 0.6±0.0 sec^{-1}. Rapid rise-rapid decay mEPPs with a mean frequency of 0.4±0.0 sec^{-1} were blocked
82 by NBQX, indicating that they depended on AMPA receptors. The mEPPs remaining after the
83 NBQX block had slower rise and decay times typical of AChR and a mean frequency of 0.1±0.0
84 sec^{-1}. The mEPPs recorded in the presence of NBQX were eliminated by the additional application
85 of pancuronium. Control larvae implanted with a saline bead had a mean frequency of 1.0±0.1 sec^{-}
86 ^{1}. Because quantal content is proportional to mEPP frequency[22,23], the higher frequency of
87 glutamatergic mEPPs than cholinergic mEPPs implies larger evoked glutamate release in response
88 to ACh receptor blockade that is a feature of homeostatic presynaptic scaling. The local block of
89 AChR did not result in immunostaining for GABA (fig. S5), in agreement with the earlier reports
90 of increase in the number of neurons expressing glutamate, but not GABA or glycine, that occurs

91 following a reduction in neuronal activity[5,24]. These results show that local block of ACh receptors
92 leads to stabilization of expression and function of another excitatory transmitter, glutamate.
93

94 **Expressing exogenous GABA receptors in embryonic myocytes**

95 Embryonic *Xenopus* motor neurons express GABA as well as glutamate in their cell bodies and in
96 their axons[21] (**Suppl Fig. 6**). Ordinarily, the level of GABA decreases by 2 dpf as ChAT appears,
97 and GABA has disappeared by 3 dpf. We expressed $GABA_A$ receptors in a small number of
98 embryonic myocytes[25] to learn whether this would stabilize expression of GABA in the motor
99 neurons that innervate them. We co-injected the transcripts for $GABA_A$ receptor α1-EGFP, β2,
100 and γ2 subunits into the ventral blastomeres (V) at the 4-cell stage, to achieve assembly of
101 $GABA_ARαβγ$ receptors. Injection of α1-EGFP transcripts alone served as control, since
102 expression in this case is restricted to the cytoplasm and does not appear in the plasma membrane[26]
103 (**Suppl Fig. 7**). The GFP-tag on the α1 subunit labeled the transfected myocytes. Strikingly, at 3
104 dpf, expression of $GABA_ARαβγ$ receptors in myocytes, but not $GABA_ARα$ alone, led to
105 expression of GABA and VGAT in the nerve terminals that innervate them (**Fig. 2; Suppl Fig. 8**).
106 ChAT was coexpressed with GABA and VGAT, suggesting that the terminals are processes of
107 motor neurons (**Suppl Fig. 9, a** to **h**). Further support that the nerve terminals expressing GABA
108 and VGAT are from motor neurons came when we traced GABA-labeled axons in the myotome
109 back to spinal cord cell bodies expressing motor neuron transcription factor Hb9 (data not shown).
110 This conclusion was strengthened by observation that GABA and Hb9, as well as GAD67 and
111 ChAT, are coexpressed in neuronal cell bodies (**Suppl Fig. 9, i** to **l**). Moreover, neurons expressing
112 ChAT and GABA in their cell bodies expressed the Lim3 and not the rAldh1a2 transcription factor.
113 This result demonstrated that the motor neurons were formed during the primary wave of

114 neurogenesis and not by a population formed later (**Suppl Fig. 10**). Expression of $GABA_AR\alpha\beta\gamma$
115 stabilized the GABAergic phenotype but did not stabilize expression of VGLUT1 or glycine in
116 innervating axons (**Suppl Fig. 11**).

117

118 The expression of GABA in motor neuron axons at 2 dpf in these embryos was increased
119 specifically in axons contacting myocytes expressing $GABA_AR\alpha\beta\gamma$. Myocytes expressing
120 $GABA_AR\alpha$ did not elicit axonal GABA expression (**Suppl Fig. 12**), suggesting that GABA was
121 stabilized by the presence of the cognate postsynaptic receptor. The stabilization of GABA in
122 axons innervating $GABA_AR\alpha\beta\gamma$-expressing myocytes persisted up to 7 dpf (**Suppl Fig. 13**). To
123 further test whether $GABA_AR\alpha\beta\gamma$-expressing myocytes were specific in stabilizing the
124 presynaptic GABAergic phenotype, we removed mesoderm of 15 hr post fertilization (hpf) wild
125 type embryos and transplanted, into these hosts, 15 hpf mesoderm grafts expressing
126 $GABA_AR\alpha\beta\gamma$ or $GABA_AR\alpha$. Only axons that contacted $GABA_AR\alpha\beta\gamma$-expressing myocytes in the
127 grafts expressed GABA and ChAT, in addition to SV2 (**Suppl Fig. 14**). Thus, stabilization of
128 GABA depended on these myocytes and not on GABA expression within the spinal cord.

129

130 To assess the functional consequence of anatomical innervation by nerve terminals expressing both
131 ChAT and GABA, we recorded mEPPs from $GABA_AR\alpha\beta\gamma$-expressing myocytes at 4 dpf. We
132 observed two classes of mEPPs, distinguished on the basis of their rise and decay times and their
133 frequency[5], with a mean overall frequency of 0.8 ± 0.1 sec^{-1}. Those with faster times occurred at a
134 mean frequency of 0.6 ± 0.0 sec^{-1} and were blocked by pancuronium, showing they depended on
135 AChR. Those with slower times occurred at a mean frequency of 0.2 ± 0.0 sec^{-1} and were blocked
136 by bicuculline (**Fig. 3, a** to **f**), indicating they depended on GABA. In contrast, only a single class

137 of mEPPs at a frequency of 1.0±0.1 sec^{-1} was observed when recording from myocytes that
138 expressed $GABA_AR\alpha$.. These mEPPs had rise and decay times similar to mEPPs recorded from
139 $GABA_AR\alpha\beta\gamma$-expressing myocytes in the presence of bicuculline (**Fig. 3, g** to **j**). The results of
140 these recordings demonstrate that GABA can be functionally released from motor nerve terminals
141 and innervate myocytes that express $GABA_AR\alpha\beta\gamma$ receptors.
142
143 **Signal transduction by trans-synaptic bridges**
144 We then considered the role of trans-synaptic bridges in retrograde signaling by postsynaptic
145 receptors that regulates the stability of presynaptic transmitters[27–29]. Presynaptic neurexins and
146 postsynaptic neuroligins and dystroglycans are synaptic adhesion molecules (SAMs) that are
147 important for proper maturation and function of synaptic contacts[30]. They bridge the synaptic cleft
148 and create a potential pathway for retrograde signaling. However, in synapse formation assays,
149 SAMs induced excitatory and inhibitory presynaptic specializations at the same time[31] and did not
150 exhibit the specificity needed if trans-synaptic bridges were to be relevant to our findings. Absent
151 from these assays were the transmitter receptors and their auxiliary subunits and co-receptors. The
152 $GABA_AR\alpha\beta\gamma$ auxiliary subunit GARLH4 mediates interaction between the γ subunit of the
153 $GABA_AR\alpha\beta\gamma$ receptor and neuroligin 2, which binds to neurexin[32]. Postsynaptic expression of
154 $GABA_AR\alpha\beta$ resulted in receptors with functional properties similar to those of $GABA_AR\alpha\beta\gamma$[24],
155 but failed to stabilize presynaptic GABA. We observed that 0 of 12 $GABA_AR\alpha\beta$-expressing larvae
156 expressed GABA in motor neuron axons contacting GFP-labeled myocytes and GABA expression
157 remained restricted to the spinal cord (**Suppl Table 2**). This finding indicated that the $GABA_AR$ γ
158 subunit of the $GABA_AR\alpha\beta\gamma$ receptor might act through a trans-synaptic bridge to achieve
159 presynaptic stability of the GABAergic phenotype.

To investigate directly whether trans-synaptic bridges stabilize presynaptic transmitters, we first confirmed the presence of neurexin, neuroligin (**Suppl Fig. 15**) and dystroglycans[33] at the *Xenopus* neuromuscular junction. Knocking down GARLH4 in myocytes, by injecting morpholinos into the V blastomeres (**Suppl Fig. 16** and **Suppl Fig. 17**), prevented the $GABA_AR\alpha\beta\gamma$-mediated stabilization of GABA in motor neurons (**Fig. 4, a** to **d**). This result suggested that the $GABA_AR$ γ subunit of the $GABA_AR\alpha\beta\gamma$ receptor mediates the expression of presynaptic GABA through GARLH4-neuroligin-neurexin trans-synaptic bridges. Similarly, disrupting AChR-rapsyn-Lrp4-musk-dystroglycan-neurexin trans-synaptic bridges[34,35], by injecting morpholinos into the V blastomeres to knock down the postsynaptic AChR co-receptor protein, Lrp4[36,37] (**Suppl Fig. 18**), recapitulated the destabilization and loss of ChAT that we observed in the presence of pancuronium (**Fig. 4, e** to **l**). Larvae in which Lrp4 was knocked down exhibited two classes of mEPPs at 4dpf, differing in their rise and decay times (**Suppl Fig. 19**) and their frequency, with an overall mean mEPP frequency of 0.7±0.1 sec^{-1}. Pancuronium-resistant NBQX-sensitive glutamatergic mEPPs were had a mean frequency of 0.5±0.0 sec^{-1}. Pancuronium-sensitive, NBQX-resistant cholinergic mEPPs had a mean frequency of 0.1±0.0 sec^{-1}. These cholinergic mEPPs, for which there were also fewer AChR[38], were smaller in amplitude compared to cholinergic mEPPs in larvae expressing the control morpholino (1.7±0.1 mV vs 2.7±0.1 mV; n^{mEPP}=177, N^{larvae}=7; $p<0.0001$, two-tailed t-test). mEPPs in control larvae implanted with a saline bead occurred at a mean frequency of 1.2±0.1 sec^{-1}. Pancuronium may phenocopy the effect of knocking down Lrp4 by binding to the α and γ subunits of the AChR[37] and altering the AChR-Lrp4 interaction, thereby disrupting signaling through cholinergic trans-synaptic bridges.

183 We next considered CASK (Ca^{2+}/calmodulin-activated Ser-Thr kinase) as a candidate that could
184 receive signals from the presynaptic ends of the trans-synaptic bridges and stabilize transmitter
185 expression in the motor neurons. CASK is a presynaptic membrane-associated guanylate kinase[39]
186 and transcription factor that binds to neurexin protein (**Fig. 4m**) and is present at both
187 glutamatergic[40] and GABAergic synapses[41]. CASK pre-mRNA is subject to alternative splicing
188 that yields proteins with preferences to interact with many targets[42]. Autophosphorylated CASK
189 translocates to the nucleus and induces transcription of genes essential for development[43,44].
190 Additionally, neurexin-1 competes as a CASK phosphorylation substrate, preventing CASK
191 autophosphorylation[45]. The splice variants, together with differential phosphorylation, identified
192 CASK as a potentially significant player in stabilizing presynaptic expression of different
193 neurotransmitters. We found that CASK is expressed in the myotome and spinal cord of wild type
194 *Xenopus* larvae (**Fig. 4, x** and **y;** and **Suppl Fig. 20**). Knocking down presynaptic CASK, by
195 injecting morpholinos into the D1.2 blastomeres to target the spinal cord (**Suppl Fig. 20**), disrupted
196 both AChR-mediated ChAT stabilization and $GABA_AR\alpha\beta\gamma$-mediated GABA stabilization in
197 motor neurons (**Fig. 4, n** to **w;** and **Suppl Table 1**). Knockdown of CASK, Lrp4 or GARLH4 did
198 not alter laminin expression or the extent of labelling by synaptophysin (SYN), indicating there
199 was no change in the gross morphology of the myocommatal junction or postsynaptic myocytes
200 (**Fig. 4, u** and **w** and **x;** and **Suppl Fig. 21**). However, presynaptic expression of CASK in spinal
201 nuclei and in myocommatal junctions was dependent on transmitter receptor identity **(Fig. 4, x** and
202 **y)**. In control larvae, CASK expression was distributed between the nuclei and the myocommatal
203 junctions. Disrupting the cholinergic trans-synaptic bridge by knocking down Lrp4 reduced CASK
204 expression to 30% of controls in the SYN-labeled myocommatal junctions, but not in the nuclei.
205 Introducing the $GABA_AR\alpha\beta\gamma$–mediated GABAergic trans-synaptic bridge and simultaneously

206 disrupting the cholinergic trans-synaptic bridge reduced CASK expression in the Hoechst-labeled
207 nuclei to 20% of controls, but not in the SYN-labelled myocommatal junctions. Disrupting the
208 GABAergic trans-synaptic bridge in the presence of the cholinergic trans-synaptic bridge
209 recapitulated the CASK expression observed in control larvae.
210

211 **Discussion**

212 Our results demonstrate that postsynaptic neurotransmitter receptors regulate the stability of
213 presynaptic neurotransmitters at newly formed neuromuscular junctions. This regulation is
214 achieved by retrograde signaling that operates through trans-synaptic bridges (**Fig. 4**). When one
215 bridge is disrupted by knock down of Lrp4, transmitter synthesis is reduced. When another bridge
216 is introduced by expression of $GABA_AR\alpha\beta\gamma$, transmitter synthesis is stabilized. Neurexin serves
217 as a presynaptic link of the trans-synaptic bridges, receiving postsynaptic receptor-dependent
218 signals and transmitting them through the neurexin-interacting protein CASK to achieve
219 presynaptic cholinergic or GABAergic stabilization. The receptor-dependent distribution of CASK
220 within the presynaptic neuron, coupled with its roles in scaffolding the synapse[46], organizing
221 presynaptic voltage-gated calcium channels[47,48] and regulating neuronal gene transcription[43],
222 provides a mechanism by which different postsynaptic receptors stabilize cognate neurotransmitter
223 expression through trans-synaptic bridges. This signaling system of trans-synaptic bridges shares
224 features with clustered protocadherin cell adhesion molecules[49], some of which change the nuclear
225 versus cytoplasmic distribution of β-catenin to regulate the Wnt pathway[50].
226

227 The reduction in presynaptic transmitter markers upon blockade of postsynaptic receptors is
228 consonant with features of presynaptic homeostatic plasticity, in which a compensatory increase

229 in neurotransmitter upon loss of receptor function is preceded by a compensatory change in
230 receptor subunits[14,15]. In *Xenopus* myocytes, where the AChR block cannot not be rescued by
231 alternative subunits[16], presynaptic synthesis of ACh was reduced and expression of glutamate
232 receptors in myocytes[5,51] led to stabilization of presynaptic glutamate[52,53].
233
234 The demonstration that trans-synaptic bridges are involved in transmitter stabilization does not
235 preclude a role for postsynaptic diffusible factors, some of which have been shown to influence
236 synapse formation and maintenance retrogradely[54–57]. Future work will determine whether deficits
237 in postsynaptic receptors or trans-synaptic bridges contribute to reduced transmitter levels at
238 neuronal synapses in the mature nervous system and to pathological change in neurological
239 disorders.
240
241 **References**

242 1. Kwon, H.-B. & Sabatini, B. L. Glutamate induces de novo growth of functional spines in
243 developing cortex. *Nature* **474**, 100–104 (2011).
244 2. Oh, W. C., Lutzu, S., Castillo, P. E. & Kwon, H.-B. De novo synaptogenesis induced by GABA
245 in the developing mouse cortex. *Science* **353**, 1037–1040 (2016).
246 3. Mattison, H. A., Popovkina, D., Kao, J. P. Y. & Thompson, S. M. The role of glutamate in the
247 morphological and physiological development of dendritic spines. *Eur. J. Neurosci.* **39**,
248 1761–1770 (2014).
249 4. Ettorre, M. *et al.* Glutamatergic neurons induce expression of functional glutamatergic
250 synapses in primary myotubes. *PLOS ONE* **7**, e31451 (2012).

251 5. Borodinsky, L. N. & Spitzer, N. C. Activity-dependent neurotransmitter-receptor matching at
252 the neuromuscular junction. *Proc. Natl. Acad. Sci.* **104**, 335–340 (2007).
253 6. Dulcis, D. & Spitzer, N. C. Illumination controls differentiation of dopamine neurons
254 regulating behaviour. *Nature* **456**, 195–201 (2008).
255 7. Dulcis, D., Jamshidi, P., Leutgeb, S. & Spitzer, N. C. Neurotransmitter switching in the adult
256 brain regulates behavior. *Science* **340**, 449–53 (2013).
257 8. Hammond-Weinberger, D. R., Wang, Y., Glavis-Bloom, A. & Spitzer, N. C. Mechanism for
258 neurotransmitter-receptor matching. *Proc. Natl. Acad. Sci. U. S. A.* (2020)
259 doi:10.1073/pnas.1916600117.
260 9. Castillo, P. E., Younts, T. J., Chávez, A. E. & Hashimotodani, Y. Endocannabinoid signaling
261 and synaptic function. *Neuron* **76**, 70–81 (2012).
262 10. Harrington, A. W. & Ginty, D. D. Long-distance retrograde neurotrophic factor signalling in
263 neurons. *Nat. Rev. Neurosci.* **14**, 177–187 (2013).
264 11. Wagh, D. A. *et al.* Bruchpilot, a protein with homology to ELKS/CAST, is required for
265 structural integrity and function of synaptic active zones in *Drosophila*. *Neuron* **49**, 833–844
266 (2006).
267 12. Frank, C. A., Kennedy, M. J., Goold, C. P., Marek, K. W. & Davis, G. W. Mechanisms
268 underlying the rapid induction and sustained expression of synaptic homeostasis. *Neuron*
269 **52**, 663–677 (2006).
270 13. Weyhersmuller, A., Hallermann, S., Wagner, N. & Eilers, J. Rapid active zone remodeling
271 during synaptic plasticity. *J. Neurosci.* **31**, 6041–6052 (2011).

272 14. Muttathukunnel, P., Frei, P., Perry, S., Dickman, D. & Müller, M. Rapid homeostatic
273 modulation of transsynaptic nanocolumn rings. *Proc. Natl. Acad. Sci.* **119**, e2119044119
274 (2022).
275 15. DiAntonio, A., Petersen, S. A., Heckmann, M. & Goodman, C. S. Glutamate receptor
276 expression regulates quantal size and quantal content at the drosophila neuromuscular
277 junction. *J. Neurosci.* **19**, 3023–3032 (1999).
278 16. Millar, N. S. & Harkness, P. C. Assembly and trafficking of nicotinic acetylcholine receptors
279 (Review). *Mol. Membr. Biol.* **25**, 279–292 (2008).
280 17. Rich, M. M., Colman, H. & Lichtman, J. W. In vivo imaging shows loss of synaptic sites from
281 neuromuscular junctions in a model of myasthenia gravis. *Neurology* **44**, 2138–2138 (1994).
282 18. Peragallo, J. H. Pediatric myasthenia gravis. *Semin. Pediatr. Neurol.* **24**, 116–121 (2017).
283 19. Engel, A. G., Shen, X.-M., Selcen, D. & Sine, S. M. Congenital myasthenic syndromes:
284 pathogenesis, diagnosis, and treatment. *Lancet Neurol.* **14**, 420–434 (2015).
285 20. Gilhus, N. E. & Verschuuren, J. J. Myasthenia gravis: subgroup classification and therapeutic
286 strategies. *Lancet Neurol.* **14**, 1023–1036 (2015).
287 21. Root, C. M., Velazquez-Ulloa, N. A., Monsalve, G. C., Minakova, E. & Spitzer, N. C.
288 Embryonically expressed GABA and glutamate drive electrical activity regulating
289 neurotransmitter specification. *J. Neurosci.* **28**, 4777–4784 (2008).
290 22. Kuno, M., Turkanis, S. A. & Weakly, J. N. Correlation between nerve terminal size and
291 transmitter release at the neuromuscular junction of the frog. *J. Physiol.* **213**, 545–556
292 (1971).

293 23. Grinnell, A. D. & Herrera, A. A. Physiological regulation of synaptic effectiveness at frog
294 neuromuscular junctions. *J. Physiol.* **307**, 301–317 (1980).
295 24. Borodinsky, L. N. *et al.* Activity-dependent homeostatic specification of transmitter
296 expression in embryonic neurons. *Nature* **429**, 523–530 (2004).
297 25. Moody, S. A. Fates of the blastomeres of the 16-cell stage *Xenopus* embryo. *Dev. Biol.* **119**,
298 560–578 (1987).
299 26. Connor, J. X., Boileau, A. J. & Czajkowski, C. A $GABA_A$ receptor α1 subunit tagged with green
300 fluorescent protein requires a β subunit for functional surface expression. *J. Biol. Chem.*
301 **273**, 28906–28911 (1998).
302 27. Dai, J., Liakath-Ali, K., Golf, S. R. & Südhof, T. C. Distinct neurexin-cerebellin complexes
303 control AMPA- and NMDA-receptor responses in a circuit-dependent manner. *eLife* **11**,
304 e78649 (2022).
305 28. Dai, J., Patzke, C., Liakath-Ali, K., Seigneur, E. & Südhof, T. C. GluD1 is a signal transduction
306 device disguised as an ionotropic receptor. *Nature* **595**, 261–265 (2021).
307 29. Gangwar, S. P. *et al.* Molecular mechanism of MDGA1: regulation of neuroligin 2:neurexin
308 trans-synaptic bridges. *Neuron* **94**, 1132-1141.e4 (2017).
309 30. Südhof, T. C. Synaptic neurexin complexes: a molecular code for the logic of neural circuits.
310 *Cell* **171**, 745–769 (2017).
311 31. Jiang, X., Sando, R. & Südhof, T. C. Multiple signaling pathways are essential for synapse
312 formation induced by synaptic adhesion molecules. **118**, (2021).
313 32. Yamasaki, T., Hoyos-Ramirez, E., Martenson, J. S., Morimoto-Tomita, M. & Tomita, S. Garlh
314 family proteins stabilize $GABA_A$ receptors at synapses. *Neuron* **93**, 1138-1152.e6 (2017).

315 33. Cohen, M., Jacobson, C., Godfrey, E., Campbell, K. & Carbonetto, S. Distribution of alpha-
316 dystroglycan during embryonic nerve-muscle synaptogenesis. *J. Cell Biol.* **129**, 1093–1101
317 (1995).
318 34. Kim, N. *et al.* Lrp4 is a receptor for agrin and forms a complex with musk. *Cell* **135**, 334–342
319 (2008).
320 35. Apel, E. D., Glass, D. J., Moscoso, L. M., Yancopoulos, G. D. & Sanes, J. R. Rapsyn is required
321 for MuSK signaling and recruits synaptic components to a MuSK-containing scaffold. *Neuron*
322 **18**, 623–635 (1997).
323 36. Yumoto, N., Kim, N. & Burden, S. J. Lrp4 is a retrograde signal for presynaptic differentiation
324 at neuromuscular synapses. *Nature* **489**, 438–442 (2012).
325 37. Fu, D. X. & Sine, S. M. Competitive antagonists bridge the alpha-gamma subunit interface of
326 the acetylcholine receptor through quaternary ammonium-aromatic interactions. *J. Biol.*
327 *Chem.* **269**, 26152–26157 (1994).
328 38. Barik, A. *et al.* Lrp4 is critical for neuromuscular junction maintenance. *J. Neurosci.* **34**,
329 13892–13905 (2014).
330 39. Tabuchi, K., Biederer, T., Butz, S. & Südhof, T. C. CASK participates in alternative tripartite
331 complexes in which mint 1 competes for binding with caskin 1, a novel CASK-binding
332 protein. *J. Neurosci.* **22**, 4264–4273 (2002).
333 40. Südhof, T. C. Neuroligins and neurexins link synaptic function to cognitive disease. *Nature*
334 **455**, 903–911 (2008).
335 41. Han, K. A. *et al.* Lar-rptps directly interact with neurexins to coordinate bidirectional
336 assembly of molecular machineries. *J. Neurosci.* **40**, 8438–8462 (2020).

337 42. Tibbe, D., Pan, Y. E., Reißner, C., Harms, F. L. & Kreienkamp, H.-J. Functional analysis of CASK
338 transcript variants expressed in human brain. *PLOS ONE* **16**, e0253223 (2021).
339 43. Hsueh, Y. P., Wang, T. F., Yang, F. C. & Sheng, M. Nuclear translocation and transcription
340 regulation by the membrane-associated guanylate kinase CASK/LIN-2. *Nat. 2000 4046775*
341 **404**, 298–302 (2000).
342 44. Huang, T.-N., Chang, H.-P. & Hsueh, Y.-P. CASK phosphorylation by PKA regulates the
343 protein-protein interactions of CASK and expression of the NMDAR2b gene. *J. Neurochem.*
344 **112**, 1562–1573 (2010).
345 45. Mukherjee, K. *et al.* CASK functions as a Mg2+-independent neurexin kinase. *Cell* **133**, 328–
346 339 (2008).
347 46. Butz, S., Okamoto, M. & Südhof, T. C. A tripartite protein complex with the potential to
348 couple synaptic vesicle exocytosis to cell adhesion in brain. *Cell* **94**, 773–782 (1998).
349 47. Maximov, A., Südhof, T. C. & Bezprozvanny, I. Association of neuronal calcium channels
350 with modular adaptor proteins. *J. Biol. Chem.* **274**, 24453–24456 (1999).
351 48. Schuh, K., Uldrijan, S., Gambaryan, S., Roethlein, N. & Neyses, L. Interaction of the plasma
352 membrane Ca2+ pump 4b/ci with the Ca2+/calmodulin-dependent membrane-associated
353 kinase CASK. *J. Biol. Chem.* **278**, 9778–9783 (2003).
354 49. Chen, W. V. & Maniatis, T. Clustered protocadherins. *Dev. Camb. Engl.* **140**, 3297–3302
355 (2013).
356 50. Pancho, A., Aerts, T., Mitsogiannis, M. D. & Seuntjens, E. Protocadherins at the Crossroad of
357 Signaling Pathways. *Front. Mol. Neurosci.* **13**, (2020).

358 51. Lambert, F. M. *et al.* Functional limb muscle innervation prior to cholinergic transmitter
359 specification during early metamorphosis in Xenopus. *eLife* **7**, e30693 (2018).
360 52. Fu, W. M., Liou, H. C., Chen, Y. H. & Wang, S. M. Coexistence of glutamate and acetylcholine
361 in the developing motoneurons. *Chin. J. Physiol.* **41**, 127–132 (1998).
362 53. Bertuzzi, M., Chang, W. & Ampatzis, K. Adult spinal motoneurons change their
363 neurotransmitter phenotype to control locomotion. *Proc. Natl. Acad. Sci. U. S. A.* **115**,
364 E9926–E9933 (2018).
365 54. Ouanounou, G., Baux, G. & Bal, T. A novel synaptic plasticity rule explains homeostasis of
366 neuromuscular transmission. *eLife* **5**, e12190 (2016).
367 55. Harish, O. E. & Poo, M. Retrograde modulation at developing neuromuscular synapses:
368 Involvement of G protein and arachidonic acid cascade. *Neuron* **9**, 1201–1209 (1992).
369 56. Tao, H. W. & Poo, M. Retrograde signaling at central synapses. *Proc. Natl. Acad. Sci.* **98**,
370 11009–11015 (2001).
371 57. Jakawich, S. K. *et al.* Local presynaptic activity gates homeostatic changes in presynaptic
372 function driven by dendritic BDNF synthesis. *Neuron* **68**, 1143–1158 (2010).
373

374 **METHODS**

375 **Animals**

376 Frogs were purchased from Nasco and Xenopus 1 and maintained on the daily light-dark cycle.
377 Experiments were performed throughout the year over a period of 4 years. No seasonal differences
378 in the data were observed. Adult female frogs were primed with 10 IU human chorionic
379 gonadotropin (HCG; Millipore Sigma) 1 week prior to collection of eggs. Testes were harvested

380 and stored in 20% fetal bovine serum or were cryopreserved till fertilization[58]. Ovulation was
381 induced by injection of 500 IU HCG 12 hr prior to egg collection and fertilization. Eggs were
382 fertilized *in vitro* and embryos developed in 0.1X Marc's modified Ringer's solution (MMR: 100
383 mM NaCl, 2 mM KCl, 1 mM $MgSO_4$, 5 mM HEPES, 0.1 mM EDTA, 2 mM $CaCl_2$, pH 7.8).
384 Developmental stages were determined from developmental tables[59,60]. All animal procedures
385 were performed in accordance with institutional guidelines and approved by the UCSD
386 Institutional Animal Care and Use Committee.

387 **Local drug delivery**

388 Spatial and temporal control of delivery of pharmacological agents was achieved using agarose
389 beads (100-200 mesh, Bio-Rad)[8,21]. Beads were washed in 2 mM Ca^{2+} medium for 3 h at 22°C,
390 replacing washing solution every 20 min, and loaded for 2 h at 4°C on a bi-directional rotator with
391 2 mM Ca^{2+} medium containing drugs 30 μM pancuronium (Fisher Scientific), or 38.9 μM curare
392 (Sigma-Aldrich), or saline (0.9% sodium chloride; stock solutions of drugs were diluted in saline).
393 Drug concentrations were 10X the concentration tested in myocyte cultures[4,5], to compensate for
394 dilution during diffusion from the bead. Beads of 120 μm diameter were selected and implanted
395 into the mesoderm (120 μm from the neural tube) ~400 μm behind the eye primordium at 20 hr
396 post fertilization (hpf) (Stage 18), allowed to develop in 0.1X MMR to 2 days post fertilization
397 (dpf) (Stage 35-36), 3 dpf (St 41), 4 dpf (St 45) or 7 dpf (St 48), and processed for
398 immunohistochemistry. Each experimental group contained 4-8 bead-implanted embryos. Only
399 myocommatal junctions $\leq$200 μm from a bead were considered for analysis.

400

401 **Plasmids and morpholinos**

402 Expression of $GABA_AR$ was achieved with $GABA_AR$ subunit plasmids for α1-EGFP, β2 and γ2
403 generated in the Czajkowski lab[26]. The $GABA_AR$ subunits were subcloned into pCS2 by
404 VectorBuilder (Santa Clara, CA)- pCS2-GABAr alpha-GFP VB180118-1043eef, pCS2 GABAr
405 beta VB180303-1004bat, pCS2 GABAr gamma VB180303-1005aab. The lissamine-tagged
406 GARLH4, Lrp4 and CASK morpholinos were supplied by GeneTools (Philomath, OR) (GARLH4
407 MO1 5'-TTCTTGTGAAGTCAACATCTTGG-3', GARLH4 MO2 5'-
408 GAGTCCTCACTCAGTATCC-3', GARLH4 negative control MO 5'-
409 GGTTCTACAACTGAAGTGTTCTT-3', Lrp4 MO 5'- CCCATAATGCCACTTCTCC-3', Lrp4
410 negative control MO 5'- CCTCTTCACCGTAATACCC-3', CASK MO 5'-
411 GGGTTTAACACCACCACAAAGGA-3', standard control oligo 5'-
412 CCTCTTACCTCAGTTACAATTTATA-3').
413
414 **Microinjections**
415 Plasmids were amplified with the QIAprep Spin miniprep kit (Qiagen) and linearized with Not1-
416 HF (New England Biolabs). α1-EGFP, β2 and γ2 capped mRNA were transcribed using the
417 mMessage mMachine SP6 kit (Invitrogen). The integrity of the mRNA was assessed using both
418 Nanodrop and agarose gel electrophoresis. On the day of microinjections, eggs were fertilized in
419 0.1X MMR and 20 min later treated in 2% cysteine (Sigma-Aldrich) to remove the jelly coat. They
420 were rinsed 10 times in 0.1X MMR and allowed to develop to the 4-cell stage in 0.1X MMR at
421 25°C. Embryos were transferred to 6% Ficoll (Sigma-Aldrich) for injections. Using a Picospritzer
422 III, α1, β2 and γ2 mRNA were co-injected into both ventral blastomeres (V) in 1:1:1 ratio along
423 with phenol red (to visualize the solution), to a total volume of 3 nl per blastomere, to target
424 expression to myocytes[61]. 6 nl of 1 mM Lrp4 MO and 1 nl or 3 nl of 1 mM GARLH4 MO or their

425 respective control morpholinos were injected into the ventral blastomeres to knockdown the
426 respective mRNAs. 6 nl of 1 mM CASK MO or its control morpholino were injected into dorsal
427 blastomeres 1.2 (D1.2) at the 16-cell stage to target expression in the spinal cord[25]. Higher doses
428 of Lrp4 MO and CASK MO were delivered to achieve widespread knock-down of the Lrp4 and
429 CASK, as strong changes in phenotype were not observed at 3 nl dose. 3 nl of 1mM GARLH4
430 labelled almost all myocytes. This dose along with GABARαβγ mRNA injection was used to test
431 the necessity of GARLH4, while the low dose of 1 nl GARLH4 MO followed 1 minute later by
432 GABARαβγ mRNA injection was used to achieve sparse labelling of myocytes with the
433 morpholino. Injected embryos were transferred to 0.1X MMR and developed at 25°C. Lissamine
434 was detected immediately post-injection, while GFP fluorescence was detected at 17 hpf (St 15)
435 as previously reported[62], and persisted up to 7 dpf (St 48).
436
437 **Whole mount immunohistochemistry**
438 Whole *Xenopus* larvae were fixed at the indicated stages of development in 4% PFA and 0.1%
439 glutaraldehyde for 1 h. After 3 washes in 1X PBS, the epidermis and head of fixed larvae were
440 removed in 1X PBS and the larvae were transferred into a 12-well plate containing blocking
441 solution (5% normal donkey serum, 1% fish gelatin, 0.5% Triton-100 in 1X PBS) for 1 h. Larvae
442 were then transferred to fresh wells containing primary antibodies diluted in 50% blocking solution
443 in 1X PBS and incubated at 4ºC for 3 d. Antibodies used were ChAT (1:500, Millipore, AB144P),
444 SV2 (1:500, Developmental Studies Hybridoma Bank, AB2315387), VGLUT1 (1:200, Millipore,
445 AB5905), GLUR1 (1:200, MilliporeSigma, MAB2263), NR1 (1:200, MilliporeSigma, MAB363),
446 GABA (1:200, Millipore, ABN131), VGAT (1:300, cytoplasmic domain, Synaptic Systems,
447 131013), GFP (1:500, Synaptic Systems, 132005), Hb9 (1:10, Developmental Studies Hybridoma

448 Bank, 81.5C10), GAD67 (1:250, Millipore, MAB5406), Glycine (1:200, Millipore, AB139), Lim3
449 (1:200, Millipore, AB3202), rAldh1a2 (1:8000, ZMBBI Columbia, CU1022), pan-Neurexin
450 (1:200, kind gift from Peter Scheiffele), pan-Neuroligin (1:200, Invitrogen, PA5-77523),
451 synaptophysin (1:200, Synaptic Systems, 101002), laminin (1:200, MilliporeSigma, L9393), Lrp4
452 (1:500, extracellular domain, generous gift from Stephan Kröger), GARLH4 (1:200, LifeSpan
453 Biosciences, LS-C170010) and CASK (1:200, Santa Cruz Biotechnology, SC-13158). After 3
454 washes in 1X PBS, larvae were incubated in the dark at 4ºC for 24 h with secondary antibodies
455 (1:500, Alexa Fluors 488, 555, 594 and 647, Jackson Immunoresearch). For CASK
456 immunostaining experiments larvae were incubated in Hoechst stain (1:8000, MilliporeSigma,
457 B2883)) for 30 mins. Following 3 washes with 1X PBS, larvae were serially dehydrated in 50%
458 methanol and 100% methanol for clearing with BABB (Benzyl alcohol:benzyl benzoate 1:2,
459 Sigma-Aldrich) for 24 h at 4ºC. After 24 h the larvae were transferred to wells containing fresh
460 BABB and reincubated for 24 h. Larvae were mounted onto slides with the side exhibiting
461 maximum expression facing up. Confocal images of whole larvae were acquired on a Leica
462 Stellaris 8 confocal microscope with 25x/0.95 water immersion objective, at a z-resolution of 0.5
463 µm, and analyzed with FIJI. For the CASK-Hoechst immunostaining experiments, images of
464 whole larvae were acquired on the Leica SP8 with 40X/1.30 oil immersion objective, at a z-
465 resolution of 0.5 µm and analyzed with FIJI. Imaging parameters were kept constant within each
466 experiment.
467
468 **Image analysis**
469 Analysis of axons running down myocommatal junctions: For bead-implantation experiments, the
470 myocommatal junction ≤200 µm anterior or posterior to the bead was analyzed. For each larva the

471 first optical slice exhibiting SV2 expression at the myocommatal junction was determined and
472 optical slices were stacked from that slice onwards to obtain 25 μm thick maximum intensity
473 projections from 50 slices, each of 0.5 μm thickness. These projections enabled examination
474 without contamination of the SV2 signal along myocommatal junctions by SV2 processes in the
475 spinal cord. The regions of interest (ROIs) for the myocommatal junctions were outlined with the
476 FIJI freehand selection tool using the SV2 signal as reference. Each maximum intensity projection
477 image was filtered for 2x background SV2, ChAT or VGLUT1 mean signal intensity and this
478 threshold was applied to all slices of the stacks. The SV2 and ChAT or VGLUT1 images were
479 converted into 8-bit format and then into binary images. The percentage area in the ROI labelled
480 with the signal was measured for SV2 and ChAT or VGLUT1. Data analysis parameters were kept
481 constant within each experiment, allowing aggregation of data from independent batches of larvae.
482 For CASK experiments the ROIs for the myocommatal junctions were outlined with the FIJI
483 freehand selection tool using the synaptophysin signal as reference, while the ROIs for nuclei were
484 outlined with the FIJI freehand selection tool using the Hoechst signal as reference.

485 Analysis of glutamate receptors on myocytes between two myocommatal junctions, spanning one
486 chevron: For each larva the first optical slice exhibiting GLUR1 or NR1 staining was determined,
487 and optical slices were stacked from that slice onwards to generate 25 μm thick maximum intensity
488 projections; these enabled examination of the myocytes in a chevron without the appearance of
489 spinal cord that could otherwise obscure visibility of the axons of motor neurons. The percentage
490 labelled area analysis of whole mount immunostained preparations included myocytes spanning
491 one chevron immediately caudal to the bead, but excluded tissue edges, damaged cells, residual
492 skin and pigment cells. Data were analyzed as described above.

493 Analysis of axons expressing GABA along the A-P axis: For GABA receptor expression
494 experiments, each larva was imaged at 4 positions along the A-P axis to cover its entire length
495 (head to tail). At each position, ~200 0.5 μm optical slices (not maximum intensity projections)
496 were acquired, thus covering the entire dorsal-ventral axis. These slices were examined one-by-
497 one to determine the number of GABA-expressing axons in the myotome. Twenty 3 dpf
498 GABARαβγ-expressing larvae were examined in this manner. When a terminal axon expressing
499 GABA was detected in the myotome of a larva, its chevron position was determined, and the
500 position of the axon was marked on a schematic of a 3 dpf larva using the ImageJ multipoint tool.
501 These points were saved as a ROI. All the ROIs were overlaid together on the 3 dpf schematic to
502 determine if there was an A-P distribution preference for these axons in the myotome. Chevrons
503 along the schematic were broadly divided into three groups for the purpose of analysis[63]: anterior
504 (light blue), chevrons 1 to 7; middle (blue), chevrons 8 to 16; and posterior (dark blue), chevrons
505 17 to 21. Chevron 21 is a composite of chevrons including and following chevron 21 in the tail,
506 which are harder to discern.

507 Analysis of GABA+Hb9+ cell bodies in the spinal cord: Images of the larvae were acquired as
508 described above. A 3D-image was created from the 0.5 μm slices. The GABA+ axon was located
509 in the myotome and traced back to the spinal cord using the 3D-Viewer and Simple Neurite Tracing
510 plugins in ImageJ.

511 Analysis of GABA, VGAT and SV2 colocalization: Colocalization was determined for each larva
512 by examining all the optical sections within a confocal stack without maximal projection.
513 Processes expressing the markers- GABA, VGAT and SV2 in at least 3 consecutive z-planes were
514 termed colocalized. The entire confocal stack was scanned optical section-by-optical section for
515 myocytes of interest, i.e. a GFP+ myocyte along the same D-V axis as the colocalized processes.

516 In each larva the first optical slice exhibiting GFP expression in myocyte of interest was
517 determined and optical slices were stacked from that slice onwards to obtain 10 μm-thick
518 maximum intensity projections from 20 slices, each of 0.5 μm thickness.
519
520 **Cell counting**
521 FIJI software was used to count fluorescent, immunolabeled ChAT+, Hb9+, Lim3+, GABA+, and
522 GAD67+ cell bodies in the spinal cord; all slices within the confocal stack through the spinal cord
523 were examined without maximal projection. Representative images are maximum intensity
524 projections of 5 consecutive slices.
525
526 **Protein extraction and ELISA**
527 ELISA assays for GFP-tagged $GABA_AR\alpha$ subunit expression in the muscle and spinal cord were
528 performed per the manufacturer's instructions (GFP ELISA Kit, Cell Biolabs). Larvae were
529 anaesthetized in 0.02% tricaine methanesulphonate (10 g/L stock solution) for 1 min, skinned and
530 gut removed using jewellers' forceps. Larvae were secured to Sylgard in a 60 mm plastic Petri
531 dish with a minutien pin (dorsal side up). The melanocyte layer covering the dorsal side (spinal
532 cord) was gently removed. 0.05% collagenase was added to the dorsal side of the larva using a
533 glass capillary, for 5 min. The collagenase was then removed and replaced with 1X PBS. The brain
534 and spinal cord were lifted out, collected into a 2 ml Eppendorf and frozen immediately in liquid
535 nitrogen. The trunk myotome was collected in another Eppendorf and frozen the same way. Thirty
536 brains and spinal cords were pooled for a single experiment to yield sufficient protein. Samples
537 were sonicated in RIPA lysis buffer (150 mM NaCl, 50 mM Tris (pH 7.4), 2 mM EDTA, 1% NP-
538 40, 0.1% SDS, 0.1 % (v/v) Protease Inhibitor) and cell debris was pelleted by centrifugation at

539 5000xg for 10 min. Protein concentration of the supernatant was estimated using the BCA method
540 (ThermoFisher).
541
542 **Mesoderm grafting**
543 Myocyte-dependent stabilization of GABA in innervating motor neuron axons was assessed by
544 mesoderm grafts. To obtain myocyte-specific $GABA_AR\alpha\beta\gamma$ or $GABA_AR\alpha$ expression, presomite
545 mesoderm of wild-type embryos 15 hpf (St 13-14) was replaced with presomite mesoderm explant
546 dissected from sibling embryos expressing either $GABA_AR\alpha\beta\gamma$ or $GABA_AR\alpha$ transcripts. The
547 grafting technique was similar to that previously described[64]. Briefly, embryos were manually
548 demembranated with jeweller's forceps, then incised using a tungsten needle in the posterior
549 region next to the blastopore, at the level of the presumptive tail-forming region. The neural plate
550 was cut laterally, left attached at the midline and lifted using a hair loop to free access to the
551 underlying presomitic mesoderm. The explant of presomitic mesoderm from the host was replaced
552 by a similarly-sized one from a GFP+ embryo, using jeweller's forceps. To immobilise the graft
553 and promote healing, the operated region was covered by a small glass coverslip bridge. The
554 grafted embryos were allowed to heal under these bridges until they were sealed and then moved
555 to 0.1X MMR for further development.
556
557 **Electrophysiology of mEPPs**
558 Sample preparation: 4 dpf (St 43) larvae were anaesthetized in ice cold 10% MMR. After ensuring
559 non-responsiveness to touch, a larva was transferred into a 60 mm Petri dish with ice cold external
560 solution, decapitated and the epidermis peeled back using sharp forceps to expose the trunk
561 myotome. The larva was moved to a Sylgard platform (~1 mm thick) in the same Petri dish and

562 glued laterally in place with Vetbond tissue adhesive (3M). A glass capillary was used to apply a
563 drop of Vetbond glue to Sylgard. The Sylgard platform with the larva was transferred into a
564 recording chamber containing external solution (NaCl 115 mM, KCl 4 mM, $CaCl_2$ 3 mM, $MgCl_2$
565 1 mM, HEPES 5 mM, D-Glucose 10 mM; pH 7.2, Osm 250-255).
566
567 Sharp electrode recording: G150F-3 (borosilicate: standard wall with filament, Warner
568 Instruments) capillaries were loaded with internal solution (3M KCl) through microfil/microloader
569 tips. Filled-capillaries were placed sharp side down on plasticine stuck to the edge of a shelf for
570 gravity-assisted removal of air bubbles. Glass pipettes with resistance of 54-75 MΩ were used for
571 recordings. GFP-labeled green myocytes, identified by the presence of sarcomeres visualized with
572 an upright Zeiss microscope and a water immersion 40X/0.8 objective, were impaled within 40
573 μm of the myocommatal junction for recordings. Multiclamp 7008, Clampex 10.7 software and
574 Clampfit 10.7 data interfaces were used for acquisition and analysis of miniature postsynaptic end-
575 plate potentials (mEPPs). The membrane potential was held at -60 mV with bridge balance for the
576 duration of recordings. mEPPs were recorded for a duration of 5 min, after which blockers
577 (pancuronium 1.5 μM, bicuculline 10 μM, or NBQX 20 μM) were perfused into the recording
578 chamber (2 ml/min). Following 10 min of perfusion, mEPPs were recorded in the presence of the
579 blockers to determine receptor-dependence. Blockers were judged effective when they reversibly
580 reduced the frequency and amplitude of mEPPs. The drugs were washed out for 20 min and
581 recovery mEPPs recorded to ensure the sample preparation was healthy throughout the recording.
582 The recordings from bead-implanted larvae and morpholino-injected larvae were performed in the
583 presence of 1 μM tetrodotoxin to prevent contribution of off-target effects of pancuronium or
584 NBQX. Rise times were scored from 10% to 90% of peak and decay times were determined by

585 fitting exponentials with the MiniAnalysis program (Synaptosoft Inc, Decatur, GA). The rise and
586 decay time distributions in different conditions were compared using Kolmogorov-Smirnov test
587 and considered significantly different when $P < 0.05$. Frequencies were scored as mEPPs min^{-1}.
588
589 **Western blotting**
590 Protein for Western blotting of components of trans-synaptic bridges was extracted as described
591 above except that larvae were anaesthetized on ice and RIPA lysis buffer was supplemented with
592 phosphatase inhibitors (PhosSTOP, Roche). 30 μg of total protein were loaded per well and
593 Ponceau S staining was used to check total protein levels on the membrane. Protein detection by
594 Western blotting was performed for Lrp4 (1:8000, extracellular domain, generous gift from
595 Stephan Kröger), GARLH4 (1:500, LifeSpan Biosciences, LS-C170010) and CASK (1:500, Santa
596 Cruz Biotechnology, SC-13158). The same blots were re-probed for the loading control actin
597 (1:1000, Sigma-Aldrich, A2066-100UL). Signal was detected using Clarity ECL Western
598 substrate (BioRad) and imaged on a BioRad Chemidoc Touch Imaging System.
599
600 **Statistics**
601 Values were expressed as mean ± SD. Statistical differences were analyzed using the unpaired,
602 two-tailed Student's *t-test* or one-way ANOVA or Kolmogorov-Smirnov test. The statistical test
603 used and the P values for each measurement are provided in the figure legends. $P<0.05$ was
604 considered statistically significant. All statistical analysis was performed in GraphPad Prism.
605
606 **Methods References**

607 58. Noble, A., Abu-Daya, A. & Guille, M. Cryopreservation of *Xenopus* Sperm and In Vitro
608 Fertilization Using Frozen Sperm Samples. *Cold Spring Harb. Protoc.* **2022**, pdb.prot107029
609 (2022).
610 59. *Normal table of* Xenopus laevis *(daudin): a systematical and chronological survey of the*
611 *development from the fertilized egg till the end of metamorphosis*. (Garland Pub, 1994).
612 60. Segerdell, E. *et al.* Enhanced XAO: the ontology of *Xenopus* anatomy and development
613 underpins more accurate annotation of gene expression and queries on Xenbase. *J. Biomed.*
614 *Semant.* **4**, 31 (2013).
615 61. Moody, S. A. & Kline, M. J. Segregation of fate during cleavage of frog (*Xenopus laevis*)
616 blastomeres. *Anat. Embryol. (Berl.)* **182**, 347–362 (1990).
617 62. Guemez-Gamboa, A., Xu, L., Meng, D. & Spitzer, N. C. Non-cell-autonomous mechanism of
618 activity-dependent neurotransmitter switching. *Neuron* **82**, 1004–1016 (2014).
619 63. Hartenstein, V. Early pattern of neuronal differentiation in the *Xenopus* embryonic
620 brainstem and spinal cord. *J. Comp. Neurol.* **328**, 213–231 (1993).
621 64. Gargioli, C. & Slack, J. M. W. Cell lineage tracing during *Xenopus* tail regeneration.
622 *Development* **131**, 2669–2679 (2004).
623

624 **Data availability statement**

625 The data that support the findings of this study are available from the corresponding author upon
626 request.

627

628 **Acknowledgements**

We thank all members of the Spitzer laboratory for discussions and critical feedback; K. Marek for discussions of acknowledgement signals; I. Gregor and R. Aricescu for discussions of receptor pharmacology and trans-synaptic bridges; C. Kintner for advice on *Xenopus* blastomere lineage; A. Ray and E. Park for guidance on miniature analysis; A. Glavis-Bloom, S.U. Choi and S. Malladi for technical assistance; D.K. Berg and L.R. Squire for comments on the manuscript. This work was supported by NSF 2051555 and the Overland Foundation. Some of the microscopy utilized the UCSD School of Medicine Microscopy Core, supported by NIH grant NS047101.

Author contributions

S.K.G and N.C.S conceived the study and designed the experiments with consultation and advice from H-q.L. and M.P. S.K.G. performed all the experiments. M.H. and H.T.C. performed electrophysiology experiments with S.K.G. Y.I. and L.S. contributed to the identification of motor neuron identity. J.B. and C.C. contributed $GABA_A$ receptor clones and advice regarding expression. J.B.L and L.N.B provided instruction in embryonic tissue transplantation. S.K.G. and N.C.S wrote the manuscript with contributions from all authors.

Competing interest statement

The authors declare no competing interests.

Additional information

1) Supplementary information is available for this paper.

2) Correspondence and requests for materials should be addressed to Swetha K. Godavarthi- skgodavarthi@ucsd.edu or Nicholas C. Spitzer- nspitzer@ucsd.edu

3) Peer review information Completed by Nature staff

4) Reprints and permission information are available at www.nature.com/reprints

Figures and legends

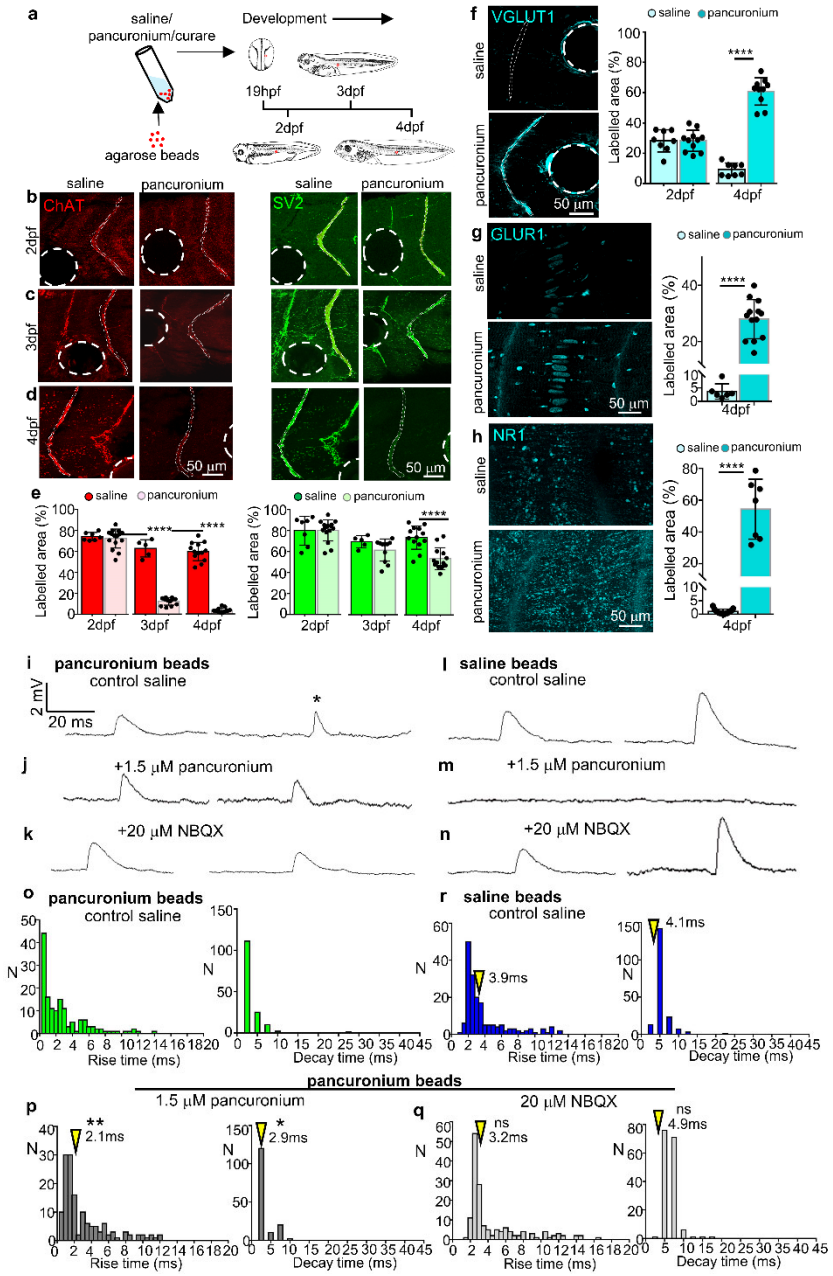

669 **Fig 1. Local block of AChR in myocytes reduces ChAT expression in innervating axons and induces a**
670 **glutamatergic phenotype.** (**a**) Experimental design. A single agarose bead loaded with pancuronium, curare, or saline
671 control was implanted into the *Xenopus* mesoderm at 19hpf. (**b-d**) Bead-implanted larvae were examined at 2dpf, 3dpf
672 and 4dpf for ChAT and SV2. Dotted lines outline myocommatal junctions analyzed for quantification of staining area.
673 Dashed lines indicate positions of beads. (**e**). Area of expression quantified for ChAT and SV2. N≥7 larvae. (**f-h**).
674 Expression and quantification of VGLUT1, GLUR1 and NR1 in 4dpf myotome of control and pancuronium-loaded
675 agarose bead-implanted larvae. N≥8 larvae. ****p<0.0001, unpaired two-tailed t-test. (**i-k**) Recordings from
676 pancuronium-bead-implanted larvae reveal rapid rise and rapid decay AMPAR-mediated-PSP-like mEPPs (asterisk)
677 that are pancuronium-resistant and NBQX-sensitive, as well as pancuronium-sensitive and NBQX-resistant mEPPs
678 with rise and decay times similar to those described for nicotinic receptor-mediated-EPPs. (**l-n**) Recordings from saline-
679 bead-implanted larvae reveal only pancuronium-sensitive mEPPs. (**o-r**) Rise and decay time distributions for mEPPs
680 in myocytes of pancuronium-bead implanted larvae and saline-bead implanted larvae. N, number of mEPPs. >155
681 mEPPs (≥3 larvae, 4dpf) for each group. Only mEPPs with decay times fit by single exponentials were included. Resting
682 potentials were held near -60 mV. Arrowheads indicate median values. Kolmogorov-Smirnov test compared rise time
683 and decay time in (**r**) with respective rise and decay time in (**p**) and (**q**). *p<0.05, **p<0.01, ns not significant.

684

685

686

687

688

689

690

691

692

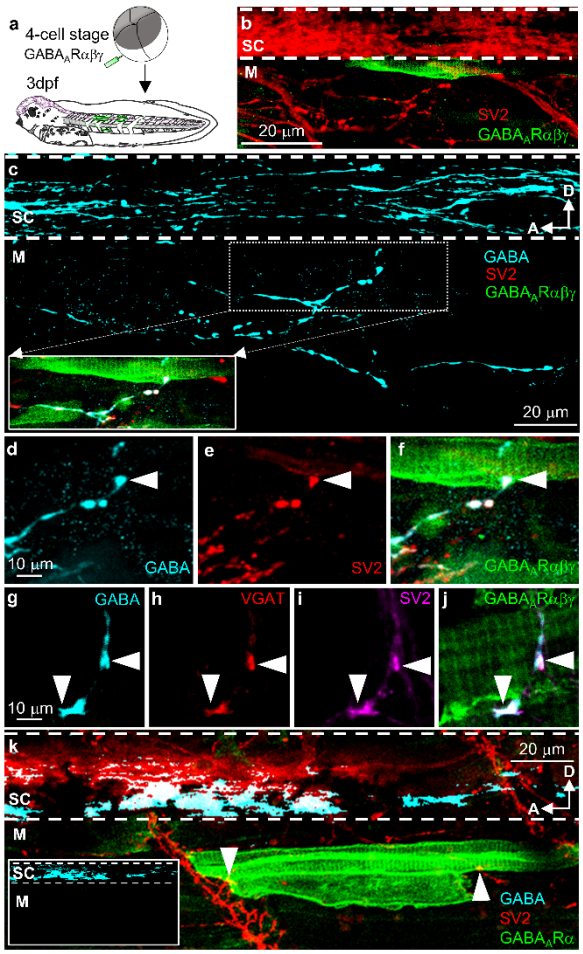

Fig 2. GABA$_A$Rαβγ expression in myocytes leads to GABA expression in axons that innervate them. (**a**) Injection of ventral blastomeres (V) with GABA$_A$Rαβγ mRNA at 4-cell stage results in myocyte-specific GABA$_A$R expression. (**b**) Sparse expression of GABA$_A$Rαβγ in the trunk myotome. SV2 labels neuronal axons in the spinal cord and in the trunk myotome. (**c**) In an expansion of the same field of view, staining for GABA reveals GABA+ axons in the spinal cord and coursing ventrally and posteriorly over the trunk myotome. *Inset:* A GABA+SV2+ axon contacts a GABA$_A$Rαβγ-expressing GFP+ myocyte (box). (**d-f**) Higher magnification of contact in (**c**) (arrowheads). (**g-j**) A GABA+VGAT+SV2+ axon contacts a different GABA$_A$Rαβγ myocyte. (**k**) Injection of ventral blastomeres (V) with GABA$_A$Rα mRNA results in sparse expression of GABA$_A$Rα in the trunk myotome. SV2+ axons contact a GABA$_A$Rα-expressing GFP+ myocyte (arrowheads). *Inset,* GABA+ axons are restricted to the spinal cord. M, trunk myotome; SC, spinal cord; D, dorsal; A, anterior. 3dpf.

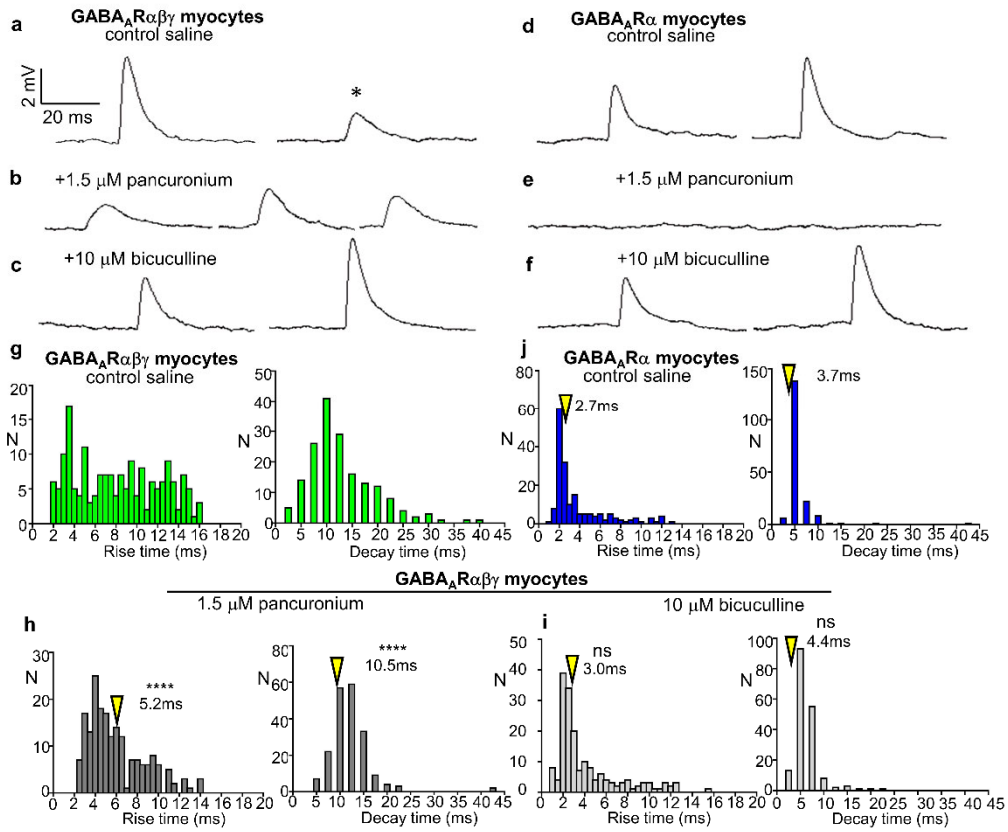

Fig 3. Neuromuscular junctions expressing GABA$_A$Rαβγ generate GABAergic and cholinergic mEPPs. (**a-c**) Recordings from GABA$_A$Rαβγ myocytes of 4dpf larvae reveal slow-rise and slow-decay GABA$_A$R-mediated mEPPs (asterisk) that are pancuronium-resistant and bicuculline-sensitive, as well as pancuronium-sensitive and bicuculline-resistant mEPPS with rise and decay times similar to those described for nicotinic receptor mediated mEPPs. (**d-f**). Rise and decay time distributions for mEPPs in GFP+ myocytes of GABA$_A$Rαβγ larvae in presence of saline, pancuronium and bicuculline. (**g-i**) Recordings from GABA$_A$Rα myocytes reveal only pancuronium-sensitive mEPPs with kinetics of nicotinic receptor mEPPs. (**j**) Rise and decay time distributions for mEPPs in GFP+ myocytes of GABA$_A$Rα larvae in presence of saline. N, number of mEPPs. >178 mEPPs ($n \geq 5$ larvae) for each group. Only mEPPs with decay times fit by single exponentials were included. Resting potentials were held near -60 mV. Arrowheads indicate median values. Kolmogorov-Smirnov test comparing rise time and decay time in (**j**) with respective rise and decay time in (**h**) and (**i**). ****$p<0.0001$, ns not significant.

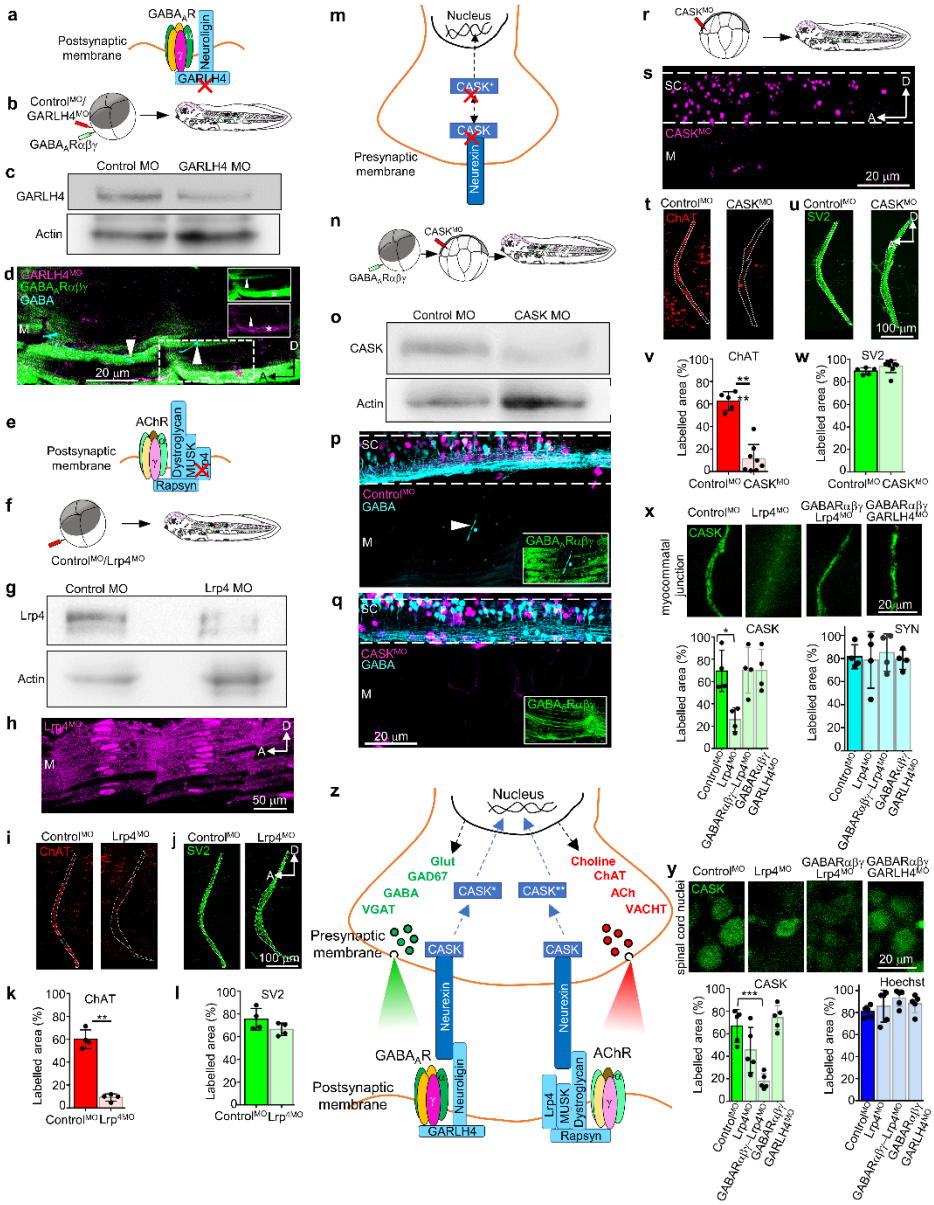

Fig 4. Receptor-driven neurotransmitter stabilization is mediated by trans-synaptic bridges. (**a**) GARLH4 links GABA$_A$Rαβγ to neuroligin in the postsynaptic membrane. (**b**) Staggered injection of ventral blastomeres (V) with GABA$_A$Rαβγ mRNA followed 1 minute later by low dose of control^{MO} or GARLH4^{MO} (3 nl of 1 mM MO). (**c**) Presence of GARLH4 and morpholino knockdown validation by Western blot. (**d**) Axons contacting GABARαβγ myocytes express GABA (arrowheads; 5/5). Axons contacting a GARLH4^{MO} GABA$_A$Rαβγ myocyte do not express GABA (asterisk, 0/12). *Insets,* individual channels for GFP (GABARαβγ) and GARLH4^{MO}. Dashed box shows the area depicted in the inserts. 3dpf. (**e**) Lrp4 links to AChR through rapsyn and to MUSK and dystroglycan in the postsynaptic membrane. (**f**) Injection of ventral blastomeres (V) with a high dose of Lrp4^{MO} or control^{MO} (6 nl of 1 mM MO). (**g**) Morpholino knockdown validation by Western blot. (**h**) Lrp4^{MO} expression in the myotome. (**i, j**) Myocommatal junctions of larvae with control

762 or Lrp4^{MO} stained for ChAT and SV2. (**k, l**) Intensity of expression of ChAT and SV2. n=4, **p=0.0092, two-tailed *t-test*.
763 3dpf. (**m**) CASK links to neurexin. (**n**) Injection of GABAR$\alpha\beta\gamma$ RNA in ventral blastomeres (V) and a high dose of
764 CASK^{MO} (6 nl of 1 mM MO) in dorsal blastomeres 1.2 (D1.2). (**o**) Presence of CASK and morpholino knockdown
765 validation by Western blot. (**p**) GABA+ axon in myotome of control^{MO} GABAR$\alpha\beta\gamma$ larva (arrowhead, 6/6). (**q**) 3dpf
766 CASK^{MO} GABA$_A$R$\alpha\beta\gamma$ larvae do not show GABA expression in the myotome (0/12). (**r**) Injection of CASK^{MO} in dorsal
767 blastomeres 1.2. (**s**) larva expressing CASK^{MO} in the SC. (**t, u**) Myocommatal junctions of larvae with control^{MO} or
768 CASK^{MO} stained for ChAT and SV2. (**v, w**) Intensity of expression of ChAT and SV2. n$\geq$5, ****p<0.0001, two-tailed *t-*
769 *test*. (**x, y**) Myocommatal junctions of larvae with control or Lrp4^{MO} or GABA$_A$R$\alpha\beta\gamma$-Lrp4^{MO} or GABA$_A$R$\alpha\beta\gamma$-GARLH4^{MO}
770 stained for CASK in synaptophysin (SYN)+ neuronal processes along the myocommatal junction and in Hoechst+
771 nuclei in the spinal cord. (**x**) Intensity of expression of CASK and SYN. N=4, *p<0.01, one-way ANOVA ($F_{3,12}$=6.316,
772 p=0.0081). (**y**) Intensity of expression of CASK and Hoechst. N=5, ***p<0.0001, one-way ANOVA ($F_{3,12}$=16.5,
773 p<0.0001). 3dpf. (**z**) Summary of interactions between neurotransmitter receptors and transsynaptic bridge proteins
774 that convey retrograde signals to achieve presynaptic transmitter stabilization. n/N, larvae with GABA+ axon/total larvae
775 observed**.** Red X in **a, e** and **m**, protein knocked-down. M, myotome; SC, spinal cord; NT, neurotransmitter; D, dorsal;
776 A, anterior.